PAPER

Fabrication of ultra-smooth and oxide-free molecule-ferromagnetic metal interfaces for applications in molecular electronics under ordinary laboratory conditions†

Karuppannan Senthil kumar,[a] Li Jiang[a] and Christian A. Nijhuis[*ab]

Self-assembled monolayers of alkanethiolates on ferromagnetic metal surfaces have potential applications in molecular spintronics, but the fabrication of such structures is complicated by unwanted oxidation of the ferromagnetic metal. This paper describes the fabrication of ultra-smooth oxide-free Ni surfaces *via* template-stripping which are protected by SAMs of $S(CH_2)_{n-1}CH_3$ that are stable for 1 day in ambient environment. Our method does not require ultra-high vacuum conditions, glove-box techniques, or (redox) cleaning of the Ni surface, but can be readily applied under ordinary laboratory conditions. Passivation of the Si/SiO$_2$ template with a layer of FOTS (1*H*,1*H*,2*H*,2*H*-perfluorooctyltrichlorosilane) reduced the Ni-template interaction sufficiently enabling successful template-stripping. The Ni^{TS}–SAM interfaces were characterized by X-ray photoelectron spectroscopy (XPS) and atomic force microscopy (AFM). We found that the surfaces were ultra-flat with a root mean square surface roughness of 0.15 $\pm$ 0.05 nm over 1.0 $\times$ 1.0 μm^2 and that they were stable against oxidation for 1 day in air at room temperature. These SAMs on Ni were incorporated in SAM-based tunneling junctions of the form Ni^{TS}–SC$_n$//GaO$_x$/EGaIn to study the tunneling rate across the SAMs. The tunneling rate is highly sensitive to defects in the SAMs or the presences of oxides. We found that the charge transport properties across these junctions were indistinguishable from those junctions with formed on Au^{TS} and Ag^{TS} substrates from which we conclude that our method yields high quality Ni^{TS}–SAM interfaces suitable for applications in molecular electronics.

Introduction

Self-assembled monolayers (SAMs) of thiol-functionalized molecules on ferromagnetic metal (FM) surfaces are interesting for possible applications in molecular,[1–5] and biomolecular-spintronics.[6–8] Such studies are challenging because the formation of metal oxides has to be minimized to ensure efficient spin-dependent charge transport[1–4] and thus there is a need to have easy access to high quality, oxide free, and defect free FM electrodes. Template-stripping (TS) is a well-known technique to generate ultra-smooth and clean metal surfaces on demand.[9–12] Often, a clean and ultra-smooth silicon (Si) surface with its native layer of SiO$_2$ is used as the template onto which a thin metal film is deposited. Next, a support, *e.g.*, a glass surface, is glued against the metal and the support/glue/metal stack is stripped off the template to expose the metal

surface that had been in contact with the template when needed. Since the metal surface was in contact with the template it is protected from the ambient environment and the template serves in this regard as a protective barrier which avoids contamination and oxidation of the metal surface. Although this method works well for inert metals such as Ag, Au, Pd, or Pt, reactive metals tend to interact too strongly with the template preventing successful template-stripping.

Here, we report a method to fabricate ultra-smooth and oxide free template-stripped nickel (Ni^{TS}) surfaces that can be obtained under ordinary laboratory conditions. This method makes it possible to strip off Ni from the Si/SiO$_2$ template *via* passivation of the template with a monolayer with a low surface energy. We characterized the SAM and Ni^{TS} surfaces with X-ray photoelectron spectroscopy (XPS) to confirm successful fabrication of oxide free FM-SAM interfaces. Our method does not rely on any ultra-high vacuum (UHV) environments and/or electrochemical reduction/cleaning processes.[13–16] Prior to template-stripping, the Ni substrates can be stored in ambient conditions for a period of time of 4–6 months. To demonstrate their usefulness, we prepared good quality molecular tunneling junctions of the form Ni^{TS}–SC$_n$//GaO$_x$/EGaIn, where, the SC$_n$ is a SAM of *n*-alkanethiolates of the form of $S(CH_2)_{n-1}CH_3$ with

*a*Department of Chemistry, National University of Singapore, 3 Science Drive 3, Singapore 117543, Singapore

*b*Centre for Advanced 2D Materials and Graphene Research Centre, National University of Singapore, 6 Science Drive 2, Singapore 117546, Singapore. E-mail: christian. nijhuis@nus.edu.sg; Tel: +65 6516 2667

$n = 10–18$. The GaO$_x$/EGaIn top-electrodes have been well-characterized and EGaIn stands for eutectic mixture of Ga and In (mp = 15.7 °C) which has a self-limiting surface layer of conductive, 0.7 nm thick GaO$_x$ (predominantly consisting of Ga$_2$O$_3$).[17,18] The electrical properties of the tunnel junctions are given by eqn (1), in which tunneling processes are characterized by the exponential decay of the current density J (in A cm^{-2}) as a function of the tunneling distance d (in nm).

$$J = J_{0,V}e^{-\beta d} \tag{1}$$

where the β (nC^{-1}) is the tunneling decay coefficient and J_0 (A cm^{-2}) is the pre-exponential factor for a predefined applied bias.[19–22] The results show that the SAMs form good quality tunneling barriers on Ni^{TS} with $\beta = 1.01 \pm 0.03$ nC^{-1} and $\log_{10}|J_0| = 2.3 \pm 0.2$ A cm^{-2}; these values are well within the range of consensus values.[20–23] These junctions also show good yields (>90%) in non-shorting junctions and high precision of data with log-standard deviations of 0.3–0.5 similar to junctions with Ag or Au bottom electrodes.[19–23]

The self-assembly of alkyl/aryl thiols on FM surfaces, such as nickel (Ni),[6,13–16,24] cobalt (Co),[14,15,24,25] and iron (Fe),[14] are challenging due to the presence of the native oxide which hampers the formation of the metal-thiolate bonds. Therefore, SAMs are immobilized on FM surfaces *via* this native oxide layer using carboxylate, phosphonate, or silane, anchoring groups.[26–29] The presence of a native oxide layer, however, often forms an anti-ferromagnetic (AFM) passivation layer which hinders the re-orientation of ferromagnetic moment of the FM layer by exchange coupling lowering the performance of, for example, spin valves.[30–32] Thus, to develop fabrication methods to obtain oxide free molecular-FM interfaces are important for molecular spintronics.

Fabrication methods based on highly controlled ultra-high vacuum (UHV) environments or *in situ* electrochemical control are available.[4,5,33–36] Most electrochemical techniques are based on a two-step procedure involving removal of the native oxide by electrochemical reduction, followed by immediate substrate immersion in alkanethiol containing ethanolic solutions. During transfer of the oxide free Ni surface, metal-oxides can form as the substrates are exposed to air. For example, Bengió *et al.*[34] reported the fabrication of *n*-alkanethiolate SAMs on Ni(111) and polycrystalline Ni surfaces by the electrochemical reduction method in which the electrochemical reduction was performed under either acidic or basic aqueous conditions, while the SAM formation was carried out either *in situ* or by pulling the substrate through a top layer of neat thiol. Instead of using two separate steps and acidic or basic aqueous electrolyte, Fontanesi *et al.*[35] performed electrochemical removal of the oxide layer with the thiol precursor present in the electrolyte (1 : 0.8, ethanol : water) and reported good quality SAMs. Hoertz *et al.*[14] used three different methods for SAM formation on Ni, Co and Fe substrates, (i) glovebox techniques (freshly evaporated metal transfer to a solution of the SAM precursor without exposure to air), (ii) electrochemical reduction inside a glovebox (oxide removal by electrochemical reduction and SAM formation carried out inside the glovebox), and (iii)

deposition of metal *via* direct metal evaporation followed by a brief exposure in air before immersion into a solution with the SAM precursor. The stability of hexadecanethiolate SAM prepared by method (i) and (ii) on FMs was examined by XPS, the sulfur atom oxidized to a S=O containing species (*e.g.*, sulfonate, sulfinate, sulfone) within 2 hours of exposure to the ambient atmosphere confirmed by the appearance of S 2p peak at ~169 eV. After five days of exposure the sample contained predominantly oxidized sulfur atoms. The oxidation of Ni surfaces slows down by the presence of SAMs under atmospheric conditions. Hoertz *et al.*[14] reported, alkanethiolate SAM on Ni surface slowed down the formation of the Ni oxide by 1–2 hours using X-ray photoelectron spectroscopy (XPS). As a group, these studies show that storing of FM surfaces is challenging.

Defects in molecular tunneling junctions, such as pinholes, need to be minimized to ensure good quality tunnelling junctions and therefore the surface roughness of the FM surface needs to be kept at a minimum.[37–42] Substrates used for preparation of SAMs on Ni by electrochemical methods have typically a root mean square (rms) surface roughness of 2.5 nm over an area of 2 × 2 μm^2 which is much higher than the molecular dimensions of the SAMs they support.[35] In addition, electrochemical etching increases the rms surface roughness of, for example, Ni and Co, by about ~40%.[14] Although the roughness is usually reported in terms of rms surface roughness, the topography can also be more comprehensively analyzed to include, grain size, width of the grain boundary, presence of pinholes, and whether the grains are located in the same plane or not. The so-called bearing volume (BV, nm^3) of the surface topography includes all of these parameters but a BV analysis has been only occasionally reported.[11] In this context, TS seems to be an attractive choice to generate FM surfaces because TS produces ultra-flat surfaces, the template provides protection from the atmosphere, and clean metal surfaces are available on demand, and therefore we developed a TS procedure to generate flat and clean Ni surfaces on-demand.

Experimental details

We purchased nickel (Ni) with purity of 99.999% from Super Conductor Material, Inc (USA) and silicon wafers (100, p-type, 500 ± 25 μm) with one side polished from University Wafers (USA). The 1H,1H,2H,2H-perfluorooctyltrichlorosilane (FOTS) and alkanethiols SC$_n$ (with $n = 10, 12, 14, 16$ and 18) were purchased from Sigma-Aldrich with a purity of 98%. We purified the alkanethiols before use as reported previously.[39] The *n*-alkanethiol with $n = 6$ was purified by distillation under vacuum. The *n*-alkanethiols with $n = 10, 12, 14, 16$ and 18 were purified by column chromatography over silica gel with hexane as an eluent and then recrystallised from ethanol under an atmosphere of N$_2$ followed by quick filtration. The gallium–indium eutectic (75.5% Ga and 24.5% In by weight) was purchased from Sigma-Aldrich. The solvents were AR grade.

Fabrication of Ni^{TS} substrate

300 nm Ni was evaporated on 1H,1H,2H,2H-perfluorooctyltrichlorosilane (FOTS) functionalized Si($\langle 100 \rangle$) substrate by

e-beam evaporation. Before Ni evaporation, the silicon substrate was exposed in FOTS for 30 min at 1 mbar in vacuum desiccators. 300 nm layer of Ni was evaporated at a rate of 0.1 Å s^{-1} monitored by a quartz crystal thickness controller. We cleaned the glass slides by ultra-sonication in ethanol solution, followed by washing with ethanol, the slides were blown to dryness in a stream on N$_2$ gas. Before we glued the glass on the nickel surfaces with optical adhesive (Norland, No. 61), the glass slides were cleaned by a plasma of air for 5 min at a pressure of 5 mbar. The optical adhesive was cured for 2 hours under UV-light irradiation following previously reported methods.[9,39] In order to prevent nickel oxidation template stripping was carried out in a N$_2$ flow hood.

Formation of SAMs on Ni^{TS}

The SAMs of alkanethiolates (SC$_n$ with $n = 10, 12, 14, 16$ and 18) were prepared by immersing freshly template-stripped Ni^{TS} from the silicon wafer inside the N$_2$ flow hood into 3 mM ethanolic solutions of the alkanethiolate molecule. The SAMs were formed overnight under a N$_2$ atmosphere (Fig. 1) using previously reported methods.[43] Then the SAM-modified substrates were rinsed with ethanol and blown to dryness in a stream of N$_2$ gas.

Monolayer characterization

The surface chemical composition of the SAMs chemisorbed on Ni^{TS} substrate was characterized by XPS using well-established procedures.[44] The photoemission spectra were measured using VG ESCA lab-220i XL XPS. The system was equipped with a monochromatic Al Kα X-ray source with a photon energy of 1486.6 eV at 15 kV. The high resolution spectra were collected at a pass energy of 20 eV, with 0.1 eV steps, at a 45° take-off angle. The binding energies were corrected against the C 1s energy of 285.0 eV. The collected XPS high resolution spectra were analysed using XPS Peak fit 4.1 software using Voigt functions (30% Lorentzian and a 70% Gaussian). The background from each spectrum was subtracted using Shirley-type back grounds to remove most of the extrinsic loss structure. The SAM thickness and tilt angle were measured using angle resolved photoelectron

spectroscopy (AR-XPS). We used synchrotron-based photoelectron spectroscopy to perform the angle resolved XPS measurements at the SINS (Surface, Interface and Nanostructure Science) beamline of Singapore Synchrotron Light Source (SSLS). The measurements were carried out at room temperature under ultra-high vacuum with a base pressure of 10^{-10} mbar. We recorded S 2p spectra at different angles of from 0° to 90° to measure surface coverage and tilt angle of SAMs on Ni^{TS} surface.

Ultraviolet photoelectron spectroscopy (UPS)

We determined the work function of the Ni^{TS} surfaces with and without SAMs with UPS at the SINS beam-line.[44] The top of the valence band and work function Φ values were determined by linear extrapolation of the lower binding energy side of the HOMO peak and secondary electron cut-off to the base line.

Atomic force microscopy (AFM)

AFM images were performed in the tapping mode, using Bruker dimension Fastscan (FASTSCAN-A, resonant frequency: 1.4 MHz, force constant: 18 N m^{-1}). We used nanoscope analysis (version 1.4) software to analyse the AFM images.

Junction fabrication and data collection

The junction fabrication and data collection has been reported before.[44] Here, we give only a brief description. We used cone-shaped EGaIn tips to approach the Ni–SAM substrates and form a junction with a diameter of 20–30 μm. For each SAM, we fabricated junctions on four to five different samples and collected five to six junctions on each sample. For each junction, we first carried out 5 scans to stabilize the junction and then collected 20 traces (except for shorts), which were all used for data analysis. We defined a short when the value of J exceeded 10^2 A cm^{-2} (the compliance value of J of our instrument) during scanning (including the first 5 scans). The yield of non-shorting junctions is defined as the number of stable junctions divided by the total number of junctions. We followed the procedure for statistical analysis of the junction data as reported before.[2] Briefly, we plotted the value of $\log_{10}|J|$ at a given bias voltage in histograms and fitted Gaussians to these histograms to obtain the log-standard deviation and log-mean of the value of J. We used this procedure for all the applied biases to construct the log-average $J(V)$ curves.

Results and discussion

Fabrication of Ni^{TS} substrates

Fig. 1 shows schematically the procedure for the preparation the Ni^{TS} substrates and formation of alkanethiolate SAMs of S(CH$_2$)$_{n-1}$CH$_3$ (in short SC$_n$) on these Ni^{TS} surfaces. As a template, we tried to use a Si wafer with its native SiO$_2$ layer (Si/SiO$_2$) or an oxide free Si template. We found that the nickel cannot be stripped off successfully because Ni interacted too strongly with these templates. To be able to peel off the nickel layer from the template, the Ni-template interaction has to be minimized. Besides, physisorbed and/or chemisorbed water on the template plays a role in the formation of nickel oxides.[45] To
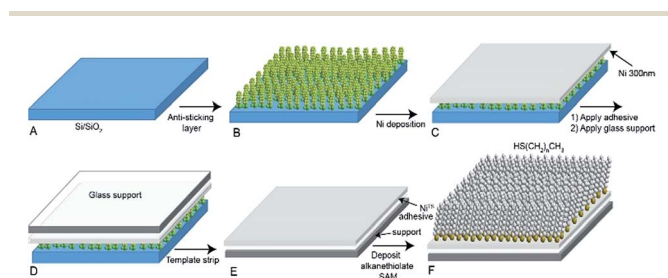

Fig. 1 Schematic illustration of the fabrication process of template-stripped Ni (Ni^{TS}) coated with a SAM. (A) On a clean Si/SiO$_2$ surface (B) FOTS was deposited followed by (C) deposition of 300 nm Ni. (D) Glass supports were glued on the Ni surface using photocurable optical adhesive. (E) After curing of the adhesive, the metal film around the glass support was cut out using a razor blade. Next, the nickel film, with its glass support, was lifted off to expose an ultra-flat Ni film (inside of a N$_2$ flow hood). (F) The Ni^{TS} surface was then immediately transferred into a solution of n-alkanethiolates.

minimize the formation of NiO bonds with the SiO_2 surface and to increase the hydrophobicity of the template, we formed a monolayer of 1H,1H,2H,2H-perfluorooctyltrichlorosilane (FOTS) on the Si/SiO_2 template via gas phase deposition for 30 min at 5×10^{-2} mbar in a vacuum desiccator (Fig. 1B). We found that this approach effectively reduced the Ni-template interaction enabling us to obtain Ni^{TS} in high yields. On the Si/SiO_2–FOTS template a layer of 300 nm thick Ni was deposited (Fig. 1C). Next, glass substrates (1×1 cm^2) were glued against the Ni layer using an epoxy glue (Norland No. 61) which was cured under UV-light irradiation following previously reported procedures (Fig. 1D).[9,11,46] Finally, we stripped of the glass/AO/Ni stacks from the Si/SiO_2–FOTS template in a N_2 flow hood to yield oxide-free Ni^{TS} surfaces that had been in contact with the template (Fig. 1E). These freshly prepared Ni^{TS} surfaces were immersed immediately (within a few seconds) into ethanolic solutions of HSC$_n$ to form SAMs overnight under a N_2 atmosphere (Fig. 1F). The samples were washed with ethanol and then dried in a stream of N_2.

Topography of the Ni^{TS} surface

We characterized the topography of the Ni^{TS} surfaces with tapping mode AFM and compared the results against Ni surfaces obtained by direct evaporation of Ni on Si/SiO_2 via e-beam evaporation (Ni^{DE}). Fig. 2 shows the AFM images of an as-deposited nickel surface Ni^{DE} (300 nm) on SiO_2/Si and Ni^{TS}. As expected, the rms surface roughness of the Ni^{TS} surfaces of 0.15 ± 0.05 nm over 1.0×1.0 μm^2 are substantially smaller than those of Ni^{DE} surfaces of 2.0 ± 0.1 nm measured over the same area. However, the topography contains more information rather than the surface roughness, such as the size of grains, the width of the grain boundaries, or the presence of pinholes. Based on previous studies, we found that exposed surface grain boundaries are the major source of defects in SAM-based tunneling junctions.[22,39,47] The exposed grain boundary area depends on the rms surface roughness (which essentially tells us whether the grains are in the same plain), grain boundary width, and size of the grains. For instance, a surface with large grains and small grain boundary widths has a smaller surface fraction of exposed grain boundaries than a surface with small grains and large grain boundary widths. Therefore, we used the bearing volume (BV), as defined in eqn (2), to determine the quality of metal surfaces
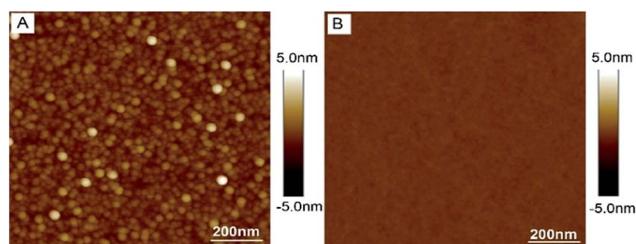
$$BV = N_{gr} \times A_{gb} \times rms \qquad (2)$$

where N_{gr} is the relative number of grains normalized by the largest grain size (where the value of N_{gr} is 1 for the surfaces with the largest grain size and the values of N_{gr} for other surfaces are the ratios of the $A_{gr}^{largest}/A_{gr}^{other}$), A_{gb} is the area of grain boundaries, and rms is the root mean square surface roughness (see ESI† and ref. 39 for the details). Generally, low BV values indicate smooth surfaces with a small fraction of exposed grain boundaries, while high BV values imply defective surfaces with a large surface fraction of exposed grain boundaries. The BV value of Ni^{TS} surface is around 2×10^5 nm^3 and that of Ni^{DE} is one order of magnitude higher (2×10^6 nm^3), which indicates the quality of Ni^{TS} is better than that of Ni^{DE} surface. The BV value of Ni^{TS} surface is similar to the high quality Au^{TS} and Ag^{TS} surfaces reported before which have been used successfully to fabricate high quality SAM-based junctions.[9,11,47]

XPS characterization of Ni^{TS} and Ni^{TS}–SAM

We measured XPS spectra of F 1s to determine whether the Ni^{TS} surface contains any residues of the FOTS passivation layer. It is well-known that the C–F bond is prone to radiation damage,[48,49] therefore we recorded the high resolution F 1s spectra before the survey scans and the other XPS measurements. Fig. S1† shows the F 1s spectrum and that no F 1s signal could detected which confirms that the Ni^{TS} surface is clean and does not contain residues (within the detection limit of our XPS) of the FOTS anti-sticking layer. We further analyzed the Ni^{TS} and Ni^{TS}–SAM surfaces by XPS to verify the chemical composition of the system with the specific aim to establish whether nickel oxide (NiO) formation was successfully prevented. Fig. 3 shows the oxygen (O 1s), nickel (Ni 2p), sulfur (S 2p), and carbon (C 1s), spectra of the Ni^{TS} and Ni^{TS}–SAM surfaces and the corresponding binding energies are summarized in Table 1. No clear signals were observed in the O 1s spectra (Fig. 3A) obtained from the Ni^{TS}–SAM substrates which confirm that no oxides
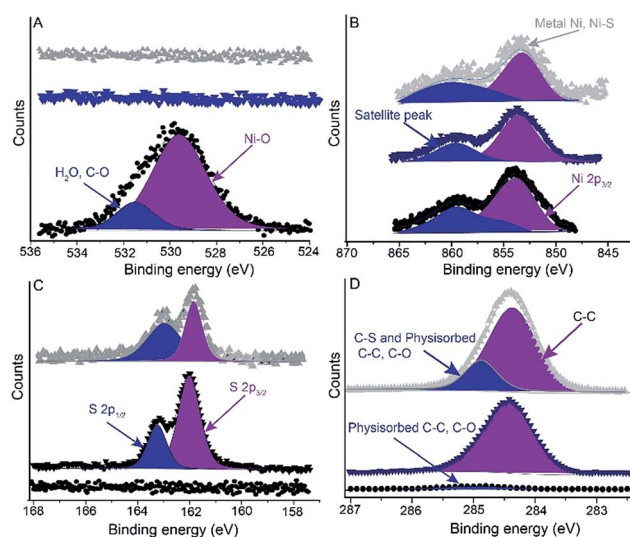

Fig. 2 Atomic force microscopy (AFM) image of (A) as deposited Ni^{DE} (300 nm) on SiO_2/Si-substrate and (B) Ni^{TS}.

Fig. 3 XPS spectra of (A) O 1s, (B) Ni 2p, (C) S 2p and (D) C 1s of the (●) bare Ni^{TS}, (▼) Ni^{TS}-C$_6$ and (▲) Ni^{TS}-C$_{14}$ substrates.

Table 1 Measured binding energies of the major core lines of SAMs on Ni^{TS} under atmospheric conditions at different time intervals

Sample	C 1s (eV)	O 1s (eV)	Ni 2p[a] (eV)	S 2p (eV)	F 1s (eV)
Ni^{TS}	285.0	529.5, 531.6	854.4, 860.0	—	—
Ni^{TS}-C_6	284.4	—	853.9, 860.3	162.0, 163.2	—
Ni^{TS}-C_{14}	284.5, 284.8	—	853.9, 860.3	161.4, 162.6	—
Ni^{TS}-C_{14} (24 h)	284.5, 284.8	—	854.0, 860.3	161.3, 162.4	—
Ni^{TS}-C_{14} (48 h)	284.5, 284.9	529.8, 530.8	854.3, 860.2	163.65	—

[a] Binding energy of Ni $2p_{3/2}$.

were present. In contrast, the bare Ni^{TS} substrates clearly show an O 1s signal at 529.5 eV corresponding to NiO. The O 1s spectra are in agreement with the Ni $2p_{3/2}$ spectra (Fig. 3B) which show that the overlapping metal-oxide (Ni–O) at 854.4 eV is absent for the Ni^{TS}–SAM samples and only a Ni–S peak at 853.9 eV can be observed. From these spectra we conclude, that within the detection limits of XPS, that a SAM on oxide free Ni^{TS} can be formed. We note, however, that the satellite peak in Fig. 3B is not completely symmetrical which could be caused by a small amount of nickel oxides.

To confirm the presence of the SAM, we measured the S 2p and C 1s spectra for from the Ni^{TS}–SAM substrates. The S 2p spectrum is dominated by a doublet with the main component at 161.4 eV ($2p_{3/2}$) and the minor component at 162.6 eV ($2p_{1/2}$). These values are typical for metal-thiolates and these data confirm the presence of the SAM. The C 1s spectra are dominated by a peak at 284.6 eV which is associate with the alkyl chain of the SAM. The weak signal at 285.0 eV for bare Ni^{TS} is due to physisorbed carbon contaminants on the Ni^{TS} surface. Although the SC_6 SAM was dominated by one peak, the SC_{14} SAM sample had an additional weak signal due to carbon contamination which likely physisorbed during transfer into the XPS chamber. From these data we conclude that both SAMs effectively prevented the formation of nickel-oxides.

Monolayer thickness, tilt angle- and work function of Ni^{TS}–SAM

We used angle resolved XPS to determine the SAM thickness, d_{SAM} in nm, on the Ni^{TS} following previously reported procedures.[39] We recorded S 2p spectra at five different angles ranging from 20° to 90° (Fig. 4A; see ESI†). The value of d_{SAM} for the SC_{14} SAMs is 1.74 ± 0.2 nm in agreement with previous reports considering a molecular length of 2.17 nm (estimated by CPK model) and a tilt angle with respect to the surface normal of 36 ± 9°.[13,34,36]

We determined the work function Φ of the Ni^{TS}–SAM and a freshly prepare native Ni^{TS} substrate by ultraviolet photoemission spectroscopy (UPS). We found that the adsorbed monolayer caused a lowering of Φ with respect to the bare Ni^{TS} surface of 0.3 eV (Fig. 4B) resulting in a similar value of Φ as of alkanethiolate SAMs on gold and silver likely due to Fermi-level pinning caused by the Ni–S bond.[50–52]

Stability of Si–FOTS/Ni and Ni^{TS}–SAM

In principle, since the Ni is in contact with the template, nickel oxides cannot form. Hence, prior to template-stripping the Ni surfaces can be stored for months without forming NiO. To test this hypothesis, we measured XPS spectra of O 1s (Fig. 5) from a Ni^{TS}–SAM surface that was stripped off the Si–FOTS/Ni template after aging of the Si–FOTS/Ni stack for six to eight months in ambient conditions. The O 1s peak was not observed for Ni^{TS}–SAM prepared on Si–FOTS/Ni aged up to six months. The Ni^{TS}–SAM formed on an 8 month old surface showed an O 1s peak at 529.5 eV which could be due to physisorbed C–O contaminations or NiO. From this observation, in line with observations made by others for Ag^{TS} surfaces,[39] we conclude that the Ni surfaces can be stored for prolonged periods of time and can be stripped of the template on demand to yield oxide free surfaces in ordinary laboratory conditions.
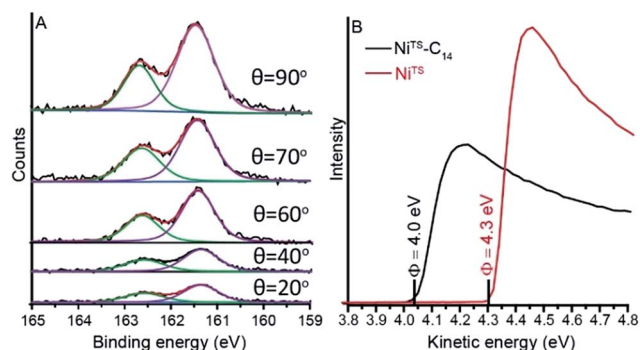

Fig. 4 (A) XPS of S 2p as a function of the take-off angle of C_{14} Ni^{TS}–SAM and (B) UPS spectra of bare Ni^{TS} and a SC_{14} SAM coated Ni^{TS}.
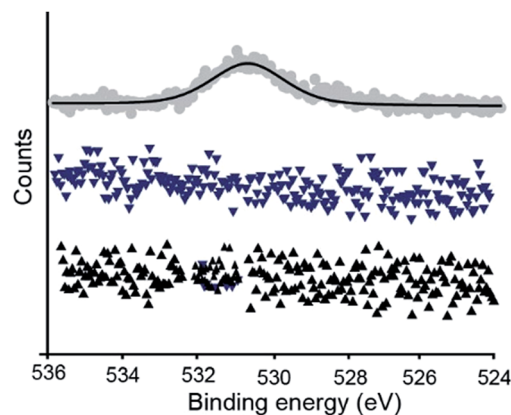

Fig. 5 XPS spectra of O 1s of Ni^{TS}–SAM substrate with the Ni^{TS} template stripped after storing for (▲) one month, (▼) 6 months and (●) 8 months of the Si–FOTS/Ni stack.

The stability of the Ni^{TS}–SAM surface upon exposure to atmospheric conditions is important to know and so we followed the rate of oxide formation on the Ni^{TS}–SAM over a period of time of 2 days under atmospheric conditions. Fig. 6A shows that after 1 h or 1 day of aging no noticeable amounts of oxides were formed. The ratio of the S 2p peak at 162.6 eV and 161.4 eV is ~2 : 1 for Ni^{TS}–SAM surface exposed in ambient conditions for 1 hour before transfer into the XPS chamber, the observed ratio is consistent with a metal-bound thiolate species (Fig. 6C). Aging for 2 days, however, caused significant degradation of the sample. The O 1s spectrum showed a peak at 529.8 eV and 530.8 eV corresponding to carbon contamination and Ni–O indicating that Ni surface started to oxidize and the typical signature of a metal-thiolate bond disappeared. We note that the carbon contamination increased with time as is evident from the decrease in the ratio of the two C 1s signals at 284 (C from the SAM) and 285 eV (C from contamination) from 2.4 to 1.1. These results show that the Ni^{TS}–SAM surfaces are stable for 1 day.

Charge transport studies

To prove that the Ni^{TS} surfaces are suitable for applications in molecular electronics, we formed molecular junctions by contacting the Ni^{TS}–SAM with cone-shaped EGaIn top-electrodes using well-established procedures.[44] Fig. 7A shows the Ni^{TS}–SC_n//GaO_x/EGaIn junction schematically. To determine β of the Ni^{TS}–SAM junctions, we prepared SAMs of SC_n (with n = 10, 12, 14, 16 and 18) immobilized on Ni^{TS} bottom-electrodes (see ESI† and Table 2). We measured the electrical properties of the Ni^{TS}–SAM junctions as a function of n (see Experimental section for details) following previously reported procedures.[22]

Fig. 7B shows the log-average $J(V)$ curves for each type of junction. We determined the value of β by fitting the data of log|J| $vs.$ n at −0.5 V (Fig. 7C) to the general tunneling equation
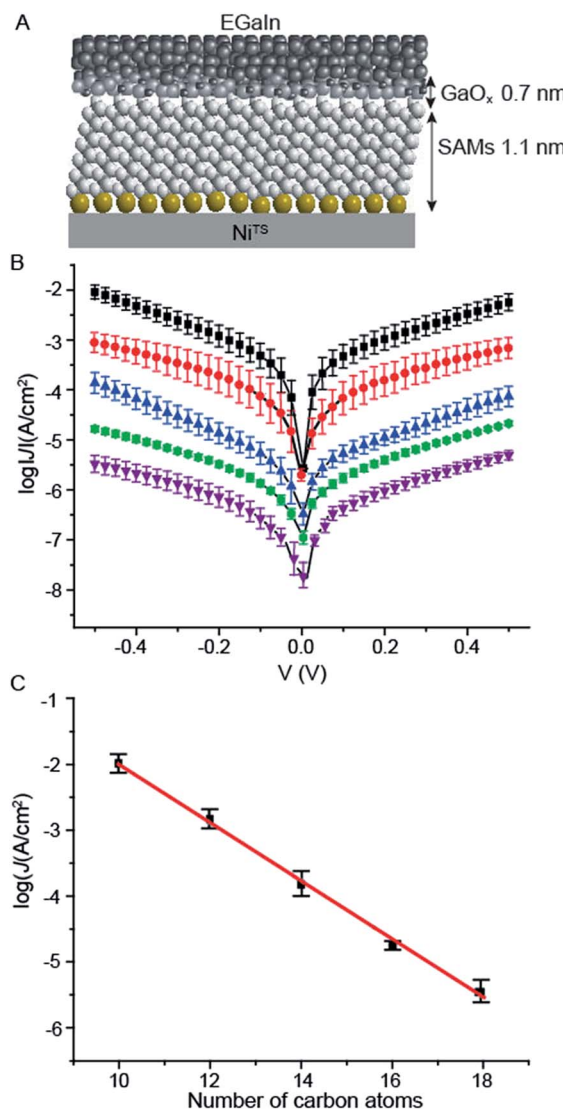

Fig. 7 (A) Schematic of the Ni^{TS}–SAM//GaO_x/EGaIn junctions, (B) plot of the log-average value J $vs.$ V of junctions with a SAM of (■) C_{10}, (●) C_{12}, (▲) C_{14}, (◆) C_{16} and (▼) C_{18} and (C) log|J| $vs.$ carbon chain length at −0.5 V. All error bars represent 95% confident intervals.
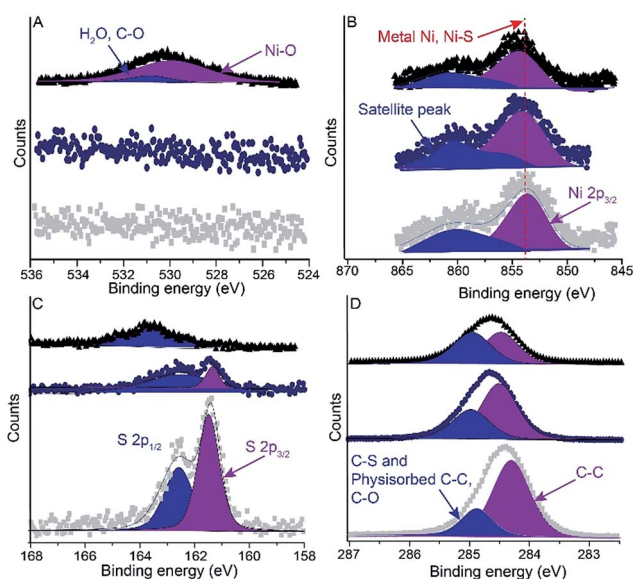

Fig. 6 XPS spectra of O 1s (A), Ni 2p (B), S 2p (C) and C 1s (D) after aging in ambient conditions of (■) Ni^{TS}-C_{14} (1 h), (●) Ni^{TS}-C_{14} (1 day) and (▲) Ni^{TS}-C_{14} (2 days).

(eqn (1)). The obtained values of $\beta = 1.01 \pm 0.03$ nC^{-1} and $\log_{10}|J_0| = 2.3 \pm 0.2$ A cm^{-2} are similar to those values obtained from junctions Au^{TS} or Ag^{TS} bottom-electrodes.[22,46] These results indicate that the dominant mechanism of charge transport across our junctions is through-bond tunneling,[22,47,53,54] where the current flows through the backbone of the alkyl chains of the SAMs. This explains why the values of J of a given molecular length of the SAM are independent of the molecular tilt angles α. In other words, the values of J across junctions with alkanethiolate SAMs on Ni^{TS} (α = ~39° ± 9°) are the same as those with SAMs on Ag^{TS} (α = ~10°) or Au^{TS} (α = ~30°) substrates.[52,53] These results indicate that the overall mechanism of charge transport is dominated by through-bond tunneling, and not through space, which is plausible since through-bond tunneling ($\beta = 0.8$ Å^{-1}) is much more efficient than through space tunnelling ($\beta = 2.9$ Å^{-1}).[20]

Table 2 Statistical analysis of $J(V)$ measurements of Ni^{TS}–SAM//GaO_x/EGaIn junctions

SAMs	No. of total junctions	No. of shorts[a]	Yield[b]	No. of stable trace	$\sigma_{\log}$[c]
$C_{10}SH$	17	2	88	375	0.44
$C_{12}SH$	17	0	100	425	0.45
$C_{14}SH$	17	1	94	400	0.50
$C_{16}SH$	14	1	93	325	0.34
$C_{18}SH$	18	2	89	400	0.47
Total	83	6	92	1925	—

[a] A short junction was defined when the value of J exceeded the compliance value of J of our instrument (100 mA) during data collection. [b] The yield is defined as the number of non-shorting junctions divided by the total number of junctions. [c] The $\sigma_{\log}$ is log-standard deviation obtained from Gaussian fitting.

Our previous studies showed that the value of β decreased from 1.0 nC^{-1} to 0.4 nC^{-1} with increasing value of BV from $\sim 10^5$ nm^3 to 10^7 nm^3.[39] Thus, here the low BV of the Ni^{TS} surfaces ($\sim 2 \times 10^5$ nm^3) ensured high quality junctions where the SAMs are good tunneling barriers. These junctions have an average yield of non-shorting junctions of 92% and good precision of data with log-standard deviations around 0.3–0.5, similar to the same junctions but with Au^{TS} and Ag^{TS} electrodes.

Conclusions

We report a procedure for direct self-assembly of n-alkanethiolate SAMs on oxide-free (within the detection limits of our XPS system) Ni^{TS} substrates without using UHV, glove box, or electrochemical reduction methods. The topography of the Ni^{TS} surface was determined by AFM and showed that the surfaces were ultra-flat and that the amount of exposed grain boundaries was small. We also showed these surfaces support densely packed SAMs of n-alkanethiolates which, in turn, stabilized the Ni^{TS} surface against oxidation in ambient conditions for 1 day. To demonstrate potential applications in molecular electronics, we incorporated the Ni^{TS} surface in Ni^{TS}–SAM//GaO_x/EGaIn junctions and measured the $J(V)$ characteristics. These measurements showed that the SAMs formed high quality tunnelling barriers and the junctions did not suffer from pin holes, with a high yield of non-shorting junctions with good reproducibility. Currently, we are investigating the Ni^{TS} surfaces in tunnelling junctions with magnetically active monolayers.

Acknowledgements

References

1 C. Barraud, P. Seneor, R. Mattana, S. Fusil, K. Bouzehouane, C. Deranlot, P. Graziosi, L. Hueso, I. Bergenti, V. Dediu, F. Petroff and A. Fert, *Nat. Phys.*, 2010, **6**, 615–620.

2 L. Schulz, L. Nuccio, M. Willis, P. Desai, P. Shakya, T. Kreouzis, V. K. Malik, C. Bernhard, F. L. Pratt, N. A. Morley, A. Suter, G. J. Nieuwenhuys, T. Prokscha, E. Morenzoni, W. P. Gillin and A. J. Drew, *Nat. Mater.*, 2011, **10**, 252.

3 P. Campiglio, R. Breitwieser, V. Repain, S. Guitteny, C. Chacon, A. Bellec, J. Lagoute, Y. Girard, S. Rousset, A. Sassella, M. Imam and S. Narasimhan, *New J. Phys.*, 2015, **17**, 063022.

4 T. Sergio, G. Marta, D. Sophie, B. Clément, B. Karim, C. Sophie, D. Cyrile, J. Eric, S. Pierre, M. Richard and P. Frédéric, *J. Phys.: Condens. Matter*, 2016, **28**, 094010.

5 P. Tyagi, E. Friebe and C. Baker, *J. Nanopart. Res.*, 2015, **17**, 452.

6 H. Einati, D. Mishra, N. Friedman, M. Sheves and R. Naaman, *Nano Lett.*, 2015, **15**, 1052–1056.

7 I. Carmeli, K. Senthil Kumar, O. Heifler, C. Carmeli and R. Naaman, *Angew. Chem., Int. Ed.*, 2014, **53**, 8953–8958.

8 R. Naaman and D. H. Waldeck, *Annu. Rev. Phys. Chem.*, 2015, **66**, 263–281.

9 E. A. Weiss, G. K. Kaufman, J. K. Kriebel, Z. Li, R. Schalek and G. M. Whitesides, *Langmuir*, 2007, **23**, 9686–9694.

10 D. Yoo, T. W. Johnson, S. Cherukulappurath, D. J. Norris and S.-H. Oh, *ACS Nano*, 2015, **9**, 10647–10654.

11 L. Jiang, T. Wang and C. A. Nijhuis, *Thin Solid Films*, 2015, **593**, 26–39.

12 S. Kumar, T. W. Johnson, C. K. Wood, T. Qu, N. J. Wittenberg, L. M. Otto, J. Shaver, N. J. Long, R. H. Victora, J. B. Edel and S. H. Oh, *ACS Appl. Mater. Interfaces*, 2016, **8**, 9319–9326.

13 A. D. Vogt, T. Han and T. P. Beebe, *Langmuir*, 1997, **13**, 3397–3403.

14 P. G. Hoertz, J. R. Niskala, P. Dai, H. T. Black and W. You, *J. Am. Chem. Soc.*, 2008, **130**, 9763–9772.

15 S. Devillers, A. Hennart, J. Delhalle and Z. Mekhalif, *Langmuir*, 2011, **27**, 14849–14860.

16 J. R. Niskala and W. You, *J. Am. Chem. Soc.*, 2009, **131**, 13202–13203.

17 C. A. Nijhuis, W. F. Reus and G. M. Whitesides, *J. Am. Chem. Soc.*, 2009, **131**, 17814–17827.

18 F. C. Simeone, H. J. Yoon, M. M. Thuo, J. R. Barber, B. Smith and G. M. Whitesides, *J. Am. Chem. Soc.*, 2013, **135**, 18131–18144.

19 H. B. Akkermann and B. D. Boer, *J. Phys.: Condens. Matter*, 2008, **20**, 013001.

20 R. L. McCreery, *Chem. Mater.*, 2004, **16**, 4477–4496.

21 K. S. Kumar, R. R. Pasula, S. Lim and C. A. Nijhuis, *Adv. Mater.*, 2016, **28**, 1824–1830.

22 L. Jiang, C. S. S. Sangeeth, A. Wan, A. Vilan and C. A. Nijhuis, *J. Phys. Chem. C*, 2015, **119**, 960–969.

23 W. F. Reus, C. A. Nijhuis, J. R. Barber, M. M. Thuo, S. Tricard and G. M. Whitesides, *J. Phys. Chem. C*, 2012, **116**, 6714–6733.

24 C. Vericat, M. E. Vela, G. Corthey, E. Pensa, E. Cortés, M. H. Fonticelli, F. Ibañez, G. E. Benitez, P. Carro and R. C. Salvarezza, *RSC Adv.*, 2014, **4**, 27730.

25 S. Pookpanratana, L. K. Lydecker, C. A. Richter and C. A. Hacker, *J. Phys. Chem. C*, 2015, **119**, 6687–6695.

26 M. Mattera, R. Torres-Cavanillas, J. P. Prieto-Ruiz, H. Prima-Garcia, S. Tatay, A. Forment-Aliaga and E. Coronado, *Langmuir*, 2015, **31**, 5311–5318.

27 S. Tatay, C. Barraud, M. Galbiati, P. Seneor, R. Mattana, K. Bouzehouane, C. Deranlot, E. Jacquet, A. Forment-Aliaga, P. Jegou, A. Fert and F. Petroff, *ACS Nano*, 2012, **6**, 8753–8757.

28 M. Galbiati, S. Tatay, S. Delprat, C. Barraud, V. Cros, E. Jacquet, F. Coloma, F. Choueikani, E. Otero, P. Ohresser, N. Haag, M. Cinchetti, M. Aeschlimann, P. Seneor, R. Mattana and F. Petroff, *Appl. Surf. Sci.*, 2015, **353**, 24–28.

29 R. Han, F. Blobner, J. Bauer, D. A. Duncan, J. V. Barth, P. Feulner and F. Allegretti, *Chem. Commun.*, 2016, **52**, 9805–9808.

30 O. Ozatay, P. G. Gowtham, K. W. Tan, J. C. Read, K. A. Mkhoyan, M. G. Thomas, G. D. Fuchs, P. M. Braganca, E. M. Ryan, K. V. Thadani, J. Silcox, D. C. Ralph and R. A. Buhrman, *Nat. Mater.*, 2008, **7**, 567–573.

31 L. De Los Santos Valladares, A. Ionescu, S. Holmes, C. H. W. Barnes, A. Bustamante Domínguez, O. Avalos Quispe, J. C. González, S. Milana, M. Barbone, A. C. Ferrari, H. Ramos and Y. Majima, *J. Vac. Sci. Technol., B*, 2014, **32**, 051808.

32 T. Y. Chung and S. Y. Hsu, *J. Phys.: Conf. Ser.*, 2009, **150**, 042063.

33 S. R. Catarelli, S. J. Higgins, W. Schwarzacher, B. W. Mao, J. W. Yan and R. J. Nichols, *Langmuir*, 2014, **30**, 14329–14336.

34 S. Bengió, M. Fonticelli, G. Benítez, A. H. Creus, P. Carro, H. Ascolani, G. Zampieri, B. Blum and R. C. Salvarezza, *J. Phys. Chem. B*, 2005, **109**, 23450–23460.

35 C. Fontanesi, F. Tassinari, F. Parenti, H. Cohen, P. C. Mondal, V. Kiran, A. Giglia, L. Pasquali and R. Naaman, *Langmuir*, 2015, **31**, 3546–3552.

36 F. Blobner, P. N. Abufager, R. Han, J. Bauer, D. A. Duncan, R. J. Maurer, K. Reuter, P. Feulner and F. Allegretti, *J. Phys. Chem. C*, 2015, **119**, 15455–15468.

37 S. Mukhopadhyay and I. Das, *Phys. Rev. Lett.*, 2006, **96**, 026601.

38 X. Chen and R. H. Victora, *Appl. Phys. Lett.*, 2007, **91**, 212104.

39 L. Yuan, L. Jiang, B. Zhang and C. A. Nijhuis, *Angew. Chem., Int. Ed.*, 2014, **53**, 3377–3381.

40 C. W. Miller, Z.-P. Li, J. Åkerman and I. K. Schuller, *Appl. Phys. Lett.*, 2007, **90**, 043513.

41 Z. S. Zhang, *J. Appl. Phys.*, 2004, **95**, 557.

42 R. H. Victora and X. Chen, *IEEE Trans. Magn.*, 2010, **46**, 702–708.

43 Z. Mekhalif, F. Laffineur, N. Couturier and J. Delhalle, *Langmuir*, 2003, **19**, 637–645.

44 L. Yuan, N. Nerngchamnong, L. Cao, H. Hamoudi, E. del Barco, M. Roemer, R. Sriramula, D. Thompson and C. A. Nijhuis, *Nat. Commun.*, 2015, **6**, 6324–6335.

45 C. H. Lee, J. H. Kim, C. Zou, I. S. Cho, J. M. Weisse, W. Nemeth, Q. Wang, A. C. van Duin, T. S. Kim and X. Zheng, *Sci. Rep.*, 2013, **3**, 2917.

46 R. C. Chiechi, E. A. Weiss, M. D. Dickey and G. M. Whitesides, *Angew. Chem., Int. Ed.*, 2008, **47**, 142–144.

47 L. Yuan, L. Jiang, D. Thompson and C. A. Nijhuis, *J. Am. Chem. Soc.*, 2014, **136**, 6554–6557.

48 S. Frey, K. Heister, M. Zharnikov and M. Grunze, *Phys. Chem. Chem. Phys.*, 2000, **2**, 1979–1987.

49 O. Zenasni, A. C. Jamison and T. R. Lee, *Soft Mater*, 2013, **9**, 6356–6370.

50 A. S. Erickson, A. Zohar and D. Cahen, *Adv. Energy Mater.*, 2014, **4**, 1301724.

51 B. Kim, S. H. Choi, X. Y. Zhu and C. D. Frisbie, *J. Am. Chem. Soc.*, 2011, **133**, 19864–19877.

52 Y. Qi, O. Yaffe, E. Tirosh, A. Vilan, D. Cahen and A. Kahn, *Chem. Phys. Lett.*, 2011, **511**, 344–347.

53 H. Song, H. Lee and T. Lee, *J. Am. Chem. Soc.*, 2007, **129**, 3806–3807.

54 K. Slowinski, R. V. Chamberlain, C. J. Miller and M. Majda, *J. Am. Chem. Soc.*, 1997, **119**, 11910–11919.